Solar Power Supply for Sensor Applications in the Field : A Guide for Environmental Scientists

Vincent Boitier, Kha Bao Khanh Cao, Bruno Estibals, Vincent Raimbault, Maxime Cauchoix, Jean-Louis Druilhe, Arnaud Elger

Solar Power Supply for Sensor Applications in the Field : A Guide for Environmental Scientists

Vincent Boitier [1,*], Kha Bao Khanh Cao [1], Bruno Estibals [1], Vincent Raimbault [1], Maxime Cauchoix[2], Jean-Louis Druilhe [3] and Arnaud Elger [3]

[1] LAAS-CNRS, Université de Toulouse, CNRS, UPS, Toulouse, France, 7 av. du colonel Roche, 31400 Toulouse, France; kha-bao-khan.cao@laas.fr (K.B.K.C.); bruno.estibals@laas.fr (B.E.); vraimbau@laas.fr (V.R.)
[2] Station d'Écologie Théorique et Expérimentale, SETE, CNRS, Moulis, France; maxime.cauchoix@sete.cnrs.fr (M.C.)
[3] Centre de Recherche sur la Biodiversité et l'Environnement, Université de Toulouse, CNRS, UPS, INPT, IRD, Toulouse, France; jean-louis.druilhe@univ-tlse3.fr (J.L.D.); arnaud.elger@toulouse-inp.fr (A.E.)
* Correspondence: vboitier@laas.fr (V.B.)

Abstract: The move toward sophisticated sensor networks in ecological applications requires a substantial amount of energy. Energy storage solutions based simply on batteries are often not sufficient to cover the energy needs, so a standalone power supply using solar energy harvesting is generally required. However, designing an appropriate solar power supply without oversizing and avoiding output power disruption all year long is not a trivial task. This paper provides a set of guidelines as well as useful information and advice for environmental researchers and other non-experts to select the right components when designing their own autonomous solar power supply for a range between 10 mW and 10 W. The design steps are compiled into a comprehensive document, free of irrelevant information yet still presenting a general overview of the solar power supply design process, in order to make this task more accessible and understandable for non-experts. The methodology for simple initial dimensioning was carried out and applied to a real-life use case by using the estimated or measured daily consumption combined with free meteorological data of the deployment site provided by various websites. Next, an hourly simulation completed the first sizing. A year of experimental results validated the methodology.

Keywords: autonomous; power supply; solar; power unit; in situ sensors; photovoltaic; battery; PV; forecast; IoT; PVGIS

---

1. Introduction

Ecological studies are increasingly moving toward high-resolution monitoring to automatically survey ecosystems in real time using the Internet-of-Things (IoT), as shown by [1]. This trend usually leads to a higher power consumption that batteries alone cannot satisfy. This means that solar energy harvesting is becoming essential. The sizing of the power supply (with or without a renewable source) is often carried out in the final part of the project, when the sensor-based instruments, data processing, and radio transmission components are virtually complete. It also arises when the user wants to switch to a completely autonomous solution that is capable of powering the device for several years without maintenance. If the design is not carried out correctly, it can lead to oversizing (extra cost, unnecessary mass) or to undersizing, which is much more damaging (foreseeable malfunctions). To the best of the authors' knowledge, there is still not a unified approach to guide non-experts on how to size an autonomous power supply.

In this case, the target audience is made up of ecologists or other field scientists who need to deploy solar energy supplies that are capable of delivering from 10 mW up to 10 W for studies in the wild. This paper aims to help them by answering (or providing some answers to) the following three questions:

1. How should the components of a standalone photovoltaic power supply be chosen?
2. What are the simple rules for interconnecting them?
3. How can the right dimensions be achieved (neither too much nor too little)?

After a description of the system used as a case study, the various components of a photovoltaic power supply are presented. The solar field is then determined. This enables the solar panel and battery to be sized, either roughly or more precisely.

1.1. Structure of a Standalone Power Supply

Primarily, it is crucial to remember the architecture of a standalone photovoltaic power supply, where one can find the following elements: a solar panel, a battery, the load to be powered (wireless sensor-based instrument), and two electronic systems, the solar charger and the output controller.

The PV panel is sized to replace the ampere-hours (Ah) in the battery consumed by the load and provide sufficient energy to overcome system losses and inefficiencies. Any additional oversizing of the PV panel is used to recharge the battery faster after periods of low solar radiation. The battery capacity has a large effect on system availability. The larger the battery, the more days of backup, and typically, the greater the system availability. The solar charger allows for the safe connection between the panel and the battery. The output regulator adjusts the voltage supplied by the battery to the voltage level required by the charge. These must be sized to withstand the panel and battery currents and voltages. Both can be integrated into a single product (dotted outline in Figure 1).

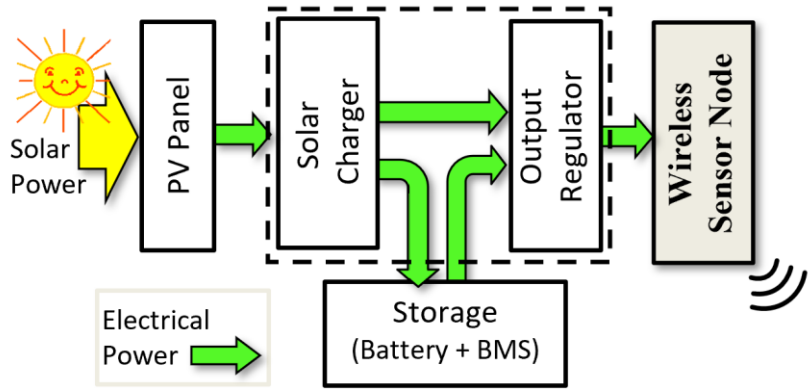

Figure 1. General architecture.

1.2. Literature Review

Many discussions within case studies already exist on the methodologies to design autonomous solar power supplies for sensor networks in nature. These systems can be used to power instruments for short- or long-distance IoT, as shown by [2]. If the system is properly sized, long-term autonomy is not a problem, unlike battery-only systems [3], unless of course the panel is covered by snow [4]. The power consumed is always kept under control [5] and can sometimes be adapted according to the level of energy available [6]. Electrical energy is stored in batteries, and very rarely in supercapacitors [7]. The impact of temperature is often noted, but battery aging has rarely been discussed. Nevertheless, the majority of existing case studies has yet to document the precise toolboxes and methodologies that can be utilized by a broader audience beyond the field of solar engineering to design their own power supply solutions. These studies often focus on a detailed analysis of specific use cases, which may not be easily accessible or applicable to a wider public outside this specialized domain.

Some papers have focused on the power consumption range of up to a few watts, as covered by this article. This range often corresponds to the use made by biologists: several sensors with fairly long acquisition times, signal processing, and radio communication [8]. For photovoltaics and batteries, voltaicsystems.com offers turnkey systems (including the box and pole), but the right panel and battery must be chosen for the job. An important step in the sizing is the establishment of the consumption budget. The power budget is measured [9] or is conducted by carrying out a daily or hourly iterative energy balance [10] based on a model of the various elements of the system.

From there, the solar panel and the battery, two key elements of the power supply, must be selected according to the local irradiation. Simple methods were presented in [11] and in [12], where both used the notion of equivalent daily hours of full sun. For example, [12] proposed sizing a solar

panel by using a worst-case based on the winter monthly weather data, with a safety factor between 10% and 40%. The authors in [13] used measured consumption data and the measured solar output of a reference panel to establish an energy balance that was simple to simulate, then they deduced the optimum panel size and the battery capacity.

Nevertheless, the sizing is often simply based on the experience of the users. Thus, the solution proposed by Libelium, dedicated to IoT with battery storage and photovoltaic recharging, is complete and has been successfully adapted by [6] in an extreme environment (glacier in Norway) with low light during the 3 winter months. However, nothing was explained regarding the choice of solar panel and battery.

Sometimes, iterative efforts on energy budget improve operation, such as those presented by [14] with a network of video cameras to study coastal erosion. As the consumption remains minimal (with an average current of 970 μA), ref. [5] showed that a fairly substantial rechargeable battery (2 years of autonomy with a 3 V 17 Ah, D-cell battery) and a 10 Wp solar panel were generically suitable for their applications without going any further into the sizing. The same applies in [15], with an end device communicating via LoRaWAN, a 4.4 Ah 12.8 V lithium battery, autonomy of more than 3 months, and was easily rechargeable with a 15 W solar panel and a simple low-end regulator. Therefore, if the weight, size, and cost constraints are lifted, oversizing is an easy and functional solution.

For field applications with systems placed in the canopy or on the water, compactness and weight become overriding factors. Furthermore, for proper sizing, if the autonomous power supply is to be provided by a photovoltaic panel (PV panel), it is necessary to have a more or less fine estimate of the solar field. Free online irradiation databases such as the NASA Power Project (power.larc.nasa.gov) (accessed on 21 10 2024) or PVGIS (re.jrc.ec.europa.eu/pvg_tools) (accessed on 21 10 2024) or paid software (PVSyst 7.4) (accessed on 21 10 2024) provide the necessary information and are easy to use. PVGIS is a simple platform for simulating the power flow of a generic solar power supply. Its implementation, however, does not facilitate any guidance to the users regarding the choice of specific hardware suitable for their intended system. Nevertheless, PVGIS remains a good starting tool for irradiance analysis, and through the user interface, access to various meteorological databases is facilitated to define the general specification of their system.

Moreover, they can be used to design and validate the dimensions of a few watts solar installation, even if they are more suitable for standalone systems such as supplying a cottage. These software packages also allow for simple shading to be taken into account (shading created by a simple volume). This is interesting, as solar panels have an important weakness that must be highlighted: A small shadow might cause a substantial loss in the harvested power [16], so the location and positioning of the panel in its environment must be carried out carefully. In applications of interest to field scientists, there is a high probability that solar panels are placed in environments with many shadows such as under a forest canopy (e.g., [17]), which can cast shadows that need to be characterized. With the shading information, it is possible to adjust the raw irradiation retrieved from the online irradiation database to arrive at a refined solar energy estimate [18]. A simulation over one year can then be performed to visualize the energy consumed and harvested over time to validate the autonomy of the system.

In this paper, a simplified version is presented. Although currently available solutions, such as PVGIS, offer tools regarding specific tasks, such as the estimation of solar energy, they are generally incomplete in the sense of supporting an overall process that leads to the optimal hardware selection in energy harvesting systems. The following work aims at presenting a generalized approach, complemented by detailed examples and case studies, assisting researchers in the optimum design of autonomous power supplies.

1.3. Application Case

The floating system presented in Figure 2 was chosen as a case study to illustrate the dimensioning method developed in this article and was developed as part of the Econnect project (econect.cnrs.fr) (accessed on 21 10 2024). Various physico-chemical water parameters were measured: pH, conductivity, O_2, redox potential (Atlas scientific sensors) as well as luminosity (VEML7700) and temperature (DS18B20) (as shown in Figure 3). The measurement cycle was 3 min. An 800L GSM SIM

module was used to send data to a server (a 2G network should suffice). This sensor node was controlled by an Arduino MEGA 2560 board.

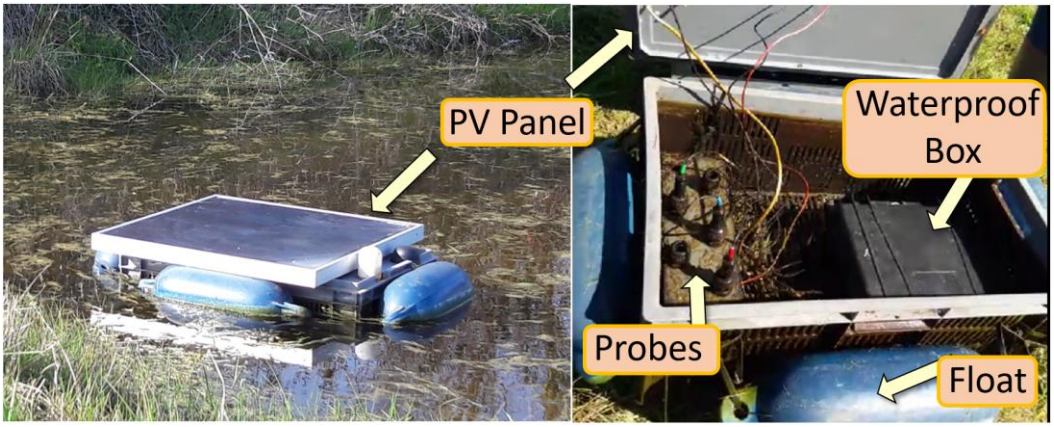

Figure 2. Aquacosme floating system for the physico-chemical water parameter measurements.

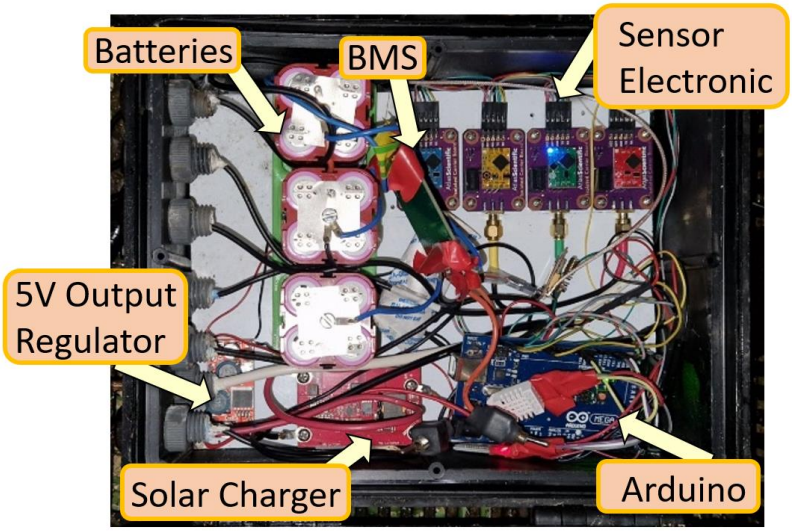

Figure 3. View of the internal components of the Aquacosme.

For the power supply, a 3S4P lithium battery pack (10.8 V, 112 Wh), a BMS board (battery management system) card for 3S lithium, a solar panel (Mono-Si, 55 Wp, *Voc* 19.8 V, 0.3 m^2), a solar charger board (BQ24650), and a 5 V output regulator (XL4015) were chosen. These choices will be explained in the rest of this paper. The system was installed in a pond in the village of Francon, near Toulouse, France, has been in place for one year, and operates perfectly.

1.4. Research Contribution

Our contribution focuses on three main areas:

1. Technical information on the various components of a photovoltaic power system and how to integrate them into a system (with only the relevant information to avoid information overload).
2. A simple methodology that uses as inputs the daily consumption, a pessimistic value of the daily irradiation and the desired autonomy, and returns the solar panel surface and battery energy.
3. A validation/optimization solution that is simple to implement with a spreadsheet, based on hourly energy consumption balance and hourly irradiation data retrieved from a free database. The simulation returns the hourly state of charge of the battery, which validates or helps to improve the previous sizing.

The goal is to allow even the non-specialist to correctly size a photovoltaic power supply.

2. Solar Power Unit Components

As illustrated in Figure 1, the autonomous solar power supply was made up of different stages. These are presented below, starting with the load consumption, and working backward to the solar panel. The following paragraphs specify the functions and present the sizing values of the solar power unit.

2.1. Consumption Analysis

The applications targeted here were sensor nodes: sensors associated with a controller (Arduino card, Raspberry Pi) and a storage (SD card) or transmission (LoRa, Sigfox, BLE, radio serial link) system. Typical voltage levels are 12 V, 5 V, 3.6 V, 3.3 V. It is important to know the maximum current absorbed and the duration of current peaks that must be supported by the upstream component as well as the average current or average power for a proper sizing of the storage stage.

Voltage, current, and power can be measured at low cost and retrieved via I2C using, for example, a DigiKey SEN0291 card. Analog current measurement can be made with a simple shunt with a high cost current clamp (Fluke i30s) or with low cost board such as a SparkFun Current Sensor SEN-13679 and a portable oscilloscope. USB power meters (Figure 4) (voltage 3.7 to 30 V, current 0 to 4 A) are also very practical, even if their sampling rate is low (2 Hz).

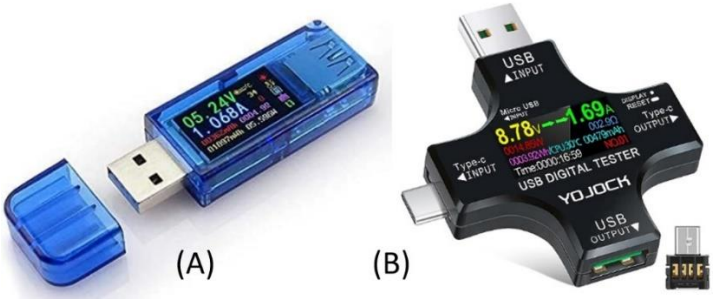

Figure 4. USB power meters. (**A**) Arceli. (**B**) Yojock.

Knowing the voltage required by the load at time t, $v_{load}(t)$ and the current drawn by the load during $i_{load}(t)$ allows us to measure the instantaneous power consumed by the load $p_{load}(t)$ using Equation (1).

$$p_{load}(t) = v_{load}(t).i_{load}(t) \quad (1)$$

By measuring the power over a period of time, we can obtain the hourly energy E_{load}^{hourly}, expressed in Wh, using Equation (2), assuming that the time is calculated in seconds.

$$E_{load}^{hourly} = \frac{1}{3600}. \int_0^{3600} p_{load}(t) \ \ dt \quad (2)$$

This equation shows the importance of measuring the power consumption over a period to obtain the energy reading and not to extrapolate the energy consumption from an instantaneous reading or from the data sheet. For our specific use case, we took measurements in situ using a laptop PC, a USB oscilloscope (2204A picoscope), a current probe (Fluke i30S with 30 turns around the core to improve resolution), and a direct voltage measurement. Experimental measurements showed a consumption of 25 Wh per day, 1.04 Wh per hour, for the 5 V-powered assembly, with current peaks of 1.4 A.

2.2. Output Stage

The main goal of the output stage is to provide a well-regulated output voltage, adapted to the loads, from the varying input voltage level of the energy storage element. There are two types to consider: switching converters (switch-mode power supplies or SMPS) or linear regulators. It is wise to select converters with certain protection features such as power cut-off in the event of load short

circuit (specified in product datasheet as OCP, over current protection) or excessive battery discharge (specified in the product data sheet as UVLO, under voltage lock out). This last function is generally incorporated in the BMS (cf. Section Battery and BMS) or in the output stage of the PV solar charger (cf. Section PWM regulators). The converter also often incorporates functions such as the inrush current limitation, thermal runaway protection, and activation via a logic input (enable pin).

2.2.1.Linear Regulator

Linear voltage regulators, also referred to as low-dropout regulators (LDO regulators), are components that provide a stable output voltage from a variable input voltage, the only limitation being that the output voltage must be smaller than the input voltage. The input current and the output current are the same (the small quiescent current could be neglected), which means that the regulator itself is dissipating some heat due to the positive voltage drops, V_{load}, between (cf. Figure 5) the input and the output pins.

This should be chosen with the desired output voltage (adjustable or not depending on the model) ~~that is~~ and capable of withstanding the maximum battery voltage and the maximum current required by the load. Quiescent current is drawn by the LDO to control its internal circuitry for proper operation where the smaller the better.

Some widely used product lines include LM317 and L4931 (fixed output voltage, with inhibit functionality).

The efficiency of the regulator (cf. Equation (3)) decreases as V_{load} increases.

$$\eta_{LDO} = \frac{p_{out}}{p_{in}} = \frac{v_{out}.i_{out}}{v_{in}.i_{in}} \approx \frac{v_{out}}{v_{in}} \quad (3)$$

If $V_{load} = 3.3\,V$ and $V_{in} = 3.6\,V$, $\eta_{LDO} \approx 92\%$, but if $V_{out} = 5\,V$ and $V_{in} = 12V$, $\eta_{LDO} \approx 42\%$. Therefore, this component is not suitable for cases where the current drawn by the load is too high or when the voltage difference between the input and output is too large.

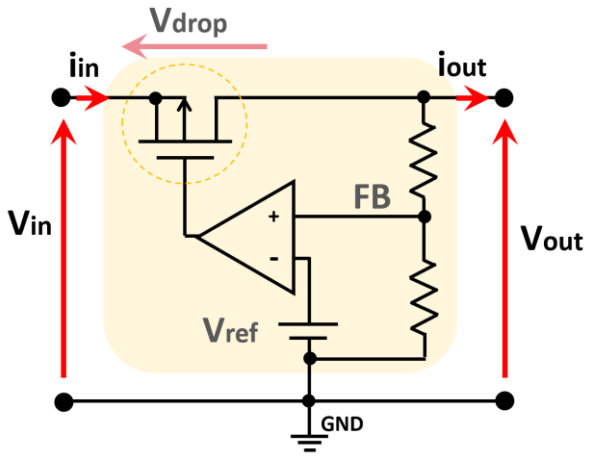

Figure 5. Simplified structure of a low-dropout regulator (LDO regulator).

2.2.2. SMPS

A switching voltage converter should be preferred due to their superior conversion efficiency and wider operating range than linear regulators. The efficiency of SMPSs (switch-mode power supplies) is around 80–90%, depending on the current load condition and the *Vout*/*Vin* ratio. The output voltage could be higher (boost, step-up converter) or lower (buck, step-down converter) than the input voltage.

The buck-boost architecture is also available, as shown in Figure 6. In this device, based on the integrated buck-boost controller XL6009, the potentiometer can be used to adjust the output voltage according to the requirements. The specifications of this specific board are a 3.8 to 48 V range for the input voltage, 1.25 to 35 V for the output voltage, and 3 A max for either the input or output current.

This should be sufficient to cover the majority of sensor-based instruments and battery solutions. For the simulation, the efficiency value must be determined based on the specific use case, with parameters taken from the technical data sheet or experimental testing.

When choosing a SMPS, it should be noted that if the converter downsizes the voltage between its output and input ($V_{out} < V_{in}$), the output current will be greater than the input current ($I_{out} > I_{in}$) and vice versa (cf. Equation (4)).

$$V_{out}.I_{out} = P_{out} = \eta_2.P_{in} = \eta_2.V_{in}.I_{in} \quad (4)$$

With η_2, the efficiency of the regulator is typically 85%.

Therefore, this stage should be chosen with the desired output voltage (adjustable or not, depending on the model) and capable of withstanding the input and output voltages and currents.

Some widely used product references are:

1. Boost: Dfrobot (SKU FIT0471) (input voltage: 0.9 to 5 V, output voltage: 5 V, 0.6 A with a typical efficiency of 85%)
2. Buck: Dfrobot (SKU DFR1015): DC-DC multi-output buck converter (3.3 V/5 V/9 V/12 V output, 5 A max).

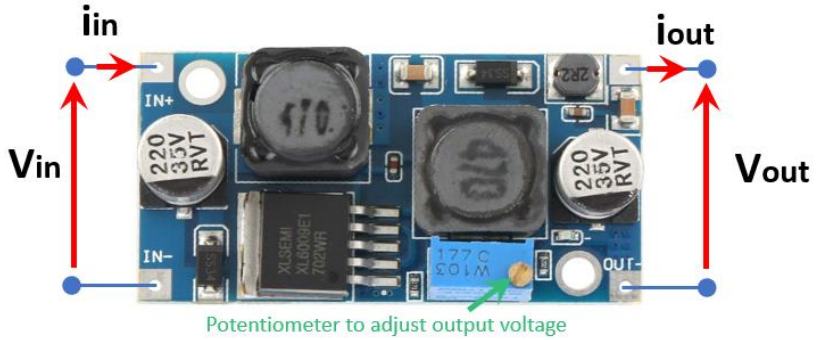

Figure 6. An example of a hobby-grade buck-boost converter found on online marketplaces.

2.3. Solar Charger

The solar charger slides in between the solar panel and batteries; its role is to ensure optimal solar energy harvesting and avoid overcharging or overdischarging of the batteries. There are also two classes of regulators that are suitable here: pulse width modulation (PWM) regulators and maximum power point tracking (MPPT) regulators based on SMPS.

2.3.1. PWM Regulators

A PWM solar regulator consists of switches, usually MOSFET, that allow or block the charging and discharging of the battery. There are two widely used architectures: serial and parallel (Figure 7). In nominal operation, the voltage of the solar panel V_{pv} is equal to and imposed by the voltage of the battery V_{bat}. This simple architecture performs well, provided that the solar panel is correctly selected according to the battery voltage (Vmp of the PV panel slightly above the nominal Vbat). This type of charger is recommended for low power applications up to 100 W.

If the battery is too discharged, switch T2 opens and disconnects the load. Note that if the output load voltage is not regulated but equal to that of the battery, an extra converter could be necessary.

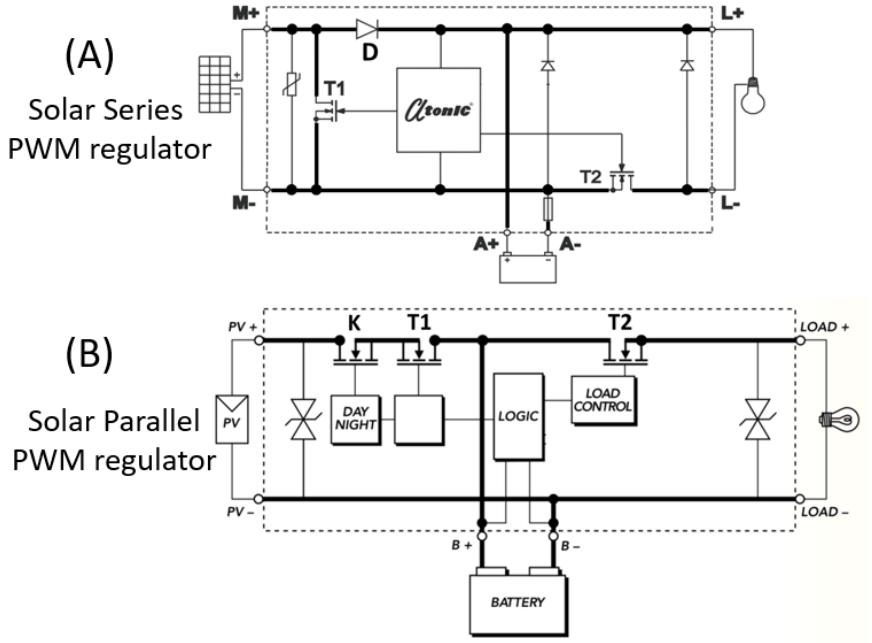

Figure 7. (**A**) Series PWM regulator and (**B**) parallel PWM regulator architectures as extracted from Steca Solsum 0606 (solaris-store.com/92-regulateur-solaire-steca-solsum-0606.html) (accessed on 21 10 2024) and Morningstar SunLight10 (solaris-shop.com/morningstar-sunlight-sl-10l-12v-pwm-charge-controller/) (accessed on 21 10 2024).

2.4.2. MPPT Regulators

Maximum power point tracking (MPPT) regulators are energy converters that can statically or dynamically set the operating point of the solar panel. The operation of the former category relies on the fact that the maximum power point (MPP) of a solar panel is found to be around 80% of its open circuit voltage. This is the case of the solar charger based on the BQ24650 integrated circuit designed by Texas Instruments, as shown in Figure 8. This board uses a resistor divider to statically set the operating point of the solar panel. Since this 80% is an approximate value and the MPP varies with temperature and irradiance, this type of converter is not optimal under varying weather conditions. For applications below 100 W, this is the more prevalent approach.

Figure 8. MPPT regulator based on the BQ24650 integrated circuit by Texas Instruments.

Meanwhile, the latter category usually employs some sort of MPPT algorithm to regularly search for MPP and optimize solar power generation, which is generally more efficient and better suits high power applications around 100 W. Examples are the SmartSolar MPPT 75/10 by Victron Energy (victronenergy.fr/solar-charge-controllers) (accessed on 21 10 2024) or the Genasun GVB-8-Pb-12V (genasun.eu/collections/genasun-lead-acid-mppts) (accessed on 21 10 2024) adapted for 12 V lead acid batteries (8 A max) that includes a real P&O MPPT algorithm.

For smaller harvested power references, all in one DFR0535, DFR0559, and DFR0580 are interesting and include the solar regulator, a connection to the battery, and the output converter to provide a 5 V output (USB).

2.4. Photovoltaic Panel

2.4.1. The Basics

The I(V) and P(V) characteristics of a PV panel vary greatly with the amount of sunlight and slightly with temperature. Usually, the technical data sheet provides parameters and curves under STC (standard test conditions): 25 °C with irradiance = 1000 W/m² (very bright sunshine). In reality, the sun varies throughout the day, as does the recoverable electrical power. If the temperature rises, the recoverable power decreases (typically −20% if the panel goes from 25 to 65 °C). The most important electrical parameters on a solar panel are:

1. The maximum power P_{MP} value in W or Wp (Watt-peak) @ ($I_{PV} = I_{MP}$, $V_{PV} = V_{MP}$);
2. The open circuit voltage V_{OC};
3. The panel short-circuit current I_{SC}.

These points are shown in Figure 9, which correspond to the ET-M53620 panel (Figure 10, item 1). This is a rigid solar panel known as "12 V" because it is suitable for charging a 12 V battery.

In general, to optimize performance in winter, the PV panel can be tilted 15° more than the latitude when the sun is low on the horizon [19].

When part of the solar panel is shaded, this can have the same effect as if all the cells were shaded, and therefore considerably reduce the electrical power that can be recovered. It is therefore advisable to avoid leaving part of the panel in the shade as much as possible.

To prevent the battery from discharging at night in the panel, a Schottky diode (low threshold that can withstand the panel current I_{SC}) is placed in series with the panel if the regulator does not have this built-in protection. The efficiency of the solar panel η_{PV} gives the quality of the panel and is given in STC, cf Equation (5).

$$\eta_{PV} = \frac{P_{MP}}{G.S} \tag{5}$$

where G is the solar irradiance in W/m² and S in m² is the panel's surface area.

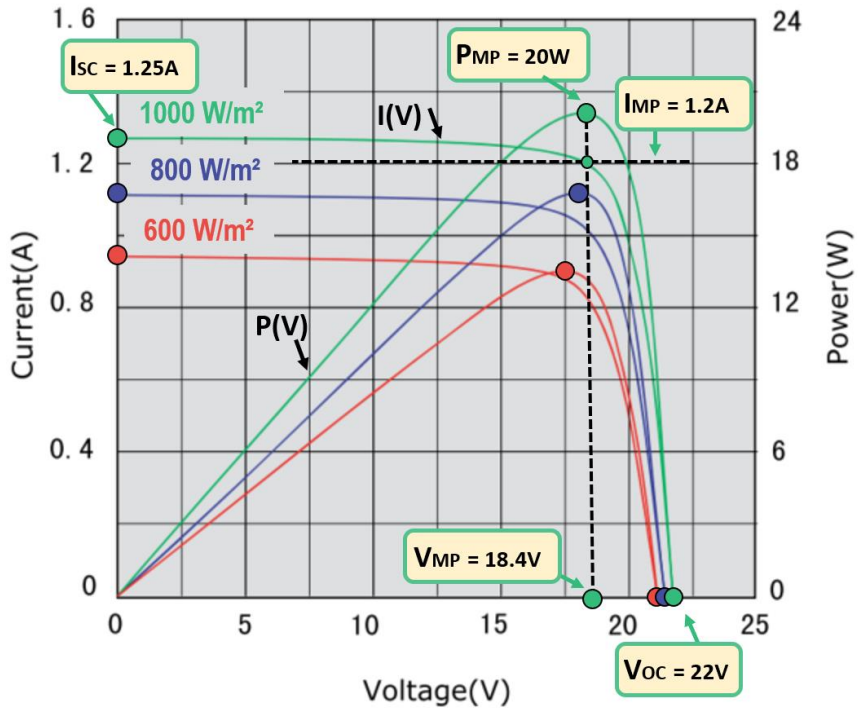

Figure 9. $I(V)$ and $P(V)$ @ T = 25 °C for different irradiances.

Figure 10. Solar panels between 5 and 20 Wp.

Table 1. Summary of the principal characteristics of several solar panels highlighted in Figure 10.

Product	Size (cm²)	Weight (kg)	P_{MP} (W)	V_{OC}/V_{MP} (W)	I_{SC}/I_{MP} (A)	USB Output
① ET-M53620 [1]	66 × 30	2.7	20	22/18.4	1.21/1.25	No
② Voltaic–ETFE [2]	22 × 15	0.19	5	7.1/6.1	0.94	No
③ BigBlue SolarPowa 10 [3]	44 × 22	0.51	10	7.75/6.35	2.21/2.157	Yes
④ Energy Flyer [4]	28 × 28	0.36	12.5	-	-	Yes, 2.4 A

[1] pdf.capenergie.fr/doc-site-isole/ET-solar-M53620.pdf (accessed on 21 10 2024) [2] voltaicsystems.com/5-watt-panel-etfe (accessed on 21 10 2024) [3] bigblue-tech.com/products/solarpowa10 (accessed on 21 10 2024) [4] solbian.eu/en/26-energy-flyer (accessed on 21 10 2024).

The STC efficiency of a good panel is around 20% in mono or polycrystalline technology. Amorphous silicon panels should be avoided (efficiency < 10%), except for indoor applications or very shaded areas. If the weight is a major factor, products such as the Solbian SP16L and SP16Q panels with 800 g for 54 W are very interesting (11 × 29 × 0.2 cm^3, $V_{OC} = 11.6$ V, $V_{MP} = 9.6$ V, $I_{SC} = 6$ A, $i_{MP} = 5.6$ A) (product page at solbian.eu/en/5-sp-series,) (accessed on 21 10 2024).

The PV area choice depends on the energy requirements. The voltage and current of the PV panel must be chosen according to the solar regulator and the battery.

Encapsulation and fixing are crucial points in the installation of a photovoltaic system to ensure that the system is watertight and durable.

2.5.2. Panel with 5 V USB Output

Some solar panels incorporate electronics and offer a 5 V USB output such as BigBlue SolarPowa10 (shown in Figure 10, item 3) (10 to 30 W), or Energy Flyer (cf. Figure 10, item 4) by Solbian (four encapsulated high-efficiency back-contact cells (12 W, 360 g) with an integrated MPPT charger self-powered by the cells and a 5 V, 2.4 A USB output.

A quality product will incorporate an MPPT function in addition to the 5 V USB output. Many products only have a simple linear regulator to obtain 5 V in the USB socket, but the expected performance is not always good. With such a regulator, the current required by the load or the battery imposes the current on the panel, which sets the panel operating point on the I(V) characteristic, but not necessarily at the optimum power.

2.5. Battery and BMS

2.5.1. Basics

The energy contained within a storage element, such as the battery shown in Figure 11, can be calculated using the following formula:

$$E = C \,.\, V \tag{6}$$

where E is the energy in Wh, capacity C in Ah, and the voltage V is in V.

Several battery technologies are available: lithium, sodium, and lead. The technologies with the highest energy density are Li-ion, LiFePO4, and LiPo. Sodium-ion batteries are a little lower down the list, and lead-acid batteries are even further down.

Figure 11. Li-ion cell, 3.7 V, 3400 mAh, 18650 form factor.

SoC and DoD

The energy remaining in a battery, expressed in %, is the state of charge (SoC). The energy consumed is the depth of discharge (DoD). The two quantities are linked by the relationship:

$$DoD\% \;=\; 100 - \;SoC\% \tag{7}$$

Therefore, for a full battery, SOC = 100% and DoD = 0%. Up to 70% DoD of a Li-ion battery can be used without significant deterioration of its useful life, as shown in [20].

Charge and Discharge Current

The capacity value is also frequently used to specify the maximum charge and discharge current ratings of a Li-ion cell. For example, a Li-ion cell with a capacity of 3000 mAh with a maximum charge current of 1 C and a discharge current of 0.5 C means that it is safe to charge and discharge this battery at maximum of 3 A and 1.5 A, respectively.

Cycling

For cycling, Na-ion and LiFePO4 are the most interesting (C > 80% initial capacity after 2000 cycles @ 100% DoD). Next comes Li-ion batteries (> 500 to 1000 cycles @ 100% DoD), then LiPo (> 300 to 500 cycles @ 100% DoD). It can be seen that the smaller the depth of discharge, the greater the number of cycles.

Temperatures

The range of operating temperatures during charging and discharging is a crucial parameter for some applications. Sodium batteries have a better operating range than lithium batteries at sub-zero temperatures for charging ([−20 , 55] °C vs. [0 , 45] °C) and discharging ([−30 , 60] °C vs. [−20 , 60] °C).

For an extreme temperature range [−30 , +125] °C, some lithium products are commercially available but at a high price (fpm-france.fr/wp-content/uploads/2015/05/Selector-guide-lithium-BD.pdf) (accessed on 21 10 2024).

Association

To obtain larger battery packs, multiple Li-ion cells of the same technology and the same manufacturer can be connected in series or parallel. For our application case, we used a 3S4P topology with 12 cells (each 3.6 V, 3 Ah), which means three branches in series each composed of four cells in parallel, giving a battery pack with a voltage of 10.8 V and an equivalent overall capacity of 12 Ah.

To increase the voltage by a factor of 1, 2, 3, or 4, the cells must be connected in series (denoted 1S, 2S, 3S, or 4S, respectively). A battery management system (BMS) must be added to protect each cell. The usual voltages for Li-ion or LiPo packs are 3.6 V, 7.2 V, 10.8 V, and 14.4 V, respectively.

If, for a given voltage, we also want to increase the capacity and therefore the stored energy, the elements must be connected in parallel. In this case, it is important to charge them all up to the same voltage levels before connection.

2.5.2. BMS

As indicated previously, for lithium or sodium batteries, a battery management system (BMS) is mandatory.

This component protects the set of cells from overvoltage during charging, undervoltage during discharging, and overcurrent during charging or discharging.

Beyond simple protection, a quality BMS also manages voltage balancing between the cells and also provides temperature monitoring to avoid overheating.

When selecting a BMS solution, it is important to consider the technology of the cells, the number of cells in series that it can handle, and its current rating according to the battery.

For the Li-ion battery pack, the BMS is usually integrated into the pack. It has two output wires for current flow and a number of fine wires so that the voltage of each cell can be measured, as shown in Figure 12. The batteries and BMS assembly are connected to pins P- and P+.

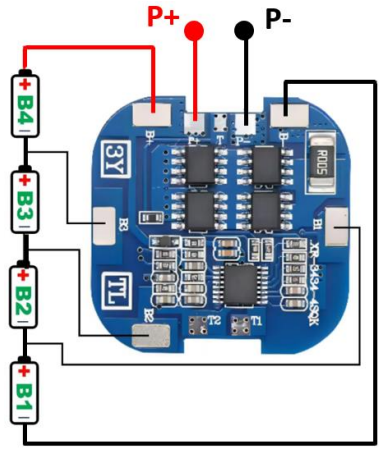

Figure 12. BMS 4S, 12.8 V, 5 A, for LiFePO4 batteries.

2.5.3. A Summary on Batteries

Currently, lithium batteries are much more widespread on the market than sodium batteries and remain the best choice in terms of energy density. However, Na-ion batteries could emerge as a compelling alternative for field applications in the coming years, as they offer a reasonably good energy density while being more eco-friendly and more performant under low temperatures compared to other technologies.

Despite its mediocre energy density, for systems where weight is not a constraint, lead-acid batteries are also suitable, and are still particularly used for voltages of 6 or 12 V and a capacity between 1 and 30 Ah. These are easily commercially available, and there is no need for a BMS. It should be noted that the maximum DOD is at best 50% for a number of cycles of 1500. The maximum continuous charge/discharge current of a lead battery is of the order of 1/10 C.

Finally, regardless of the type of battery chosen, a suitable solar charger will need to be used to comply with the charging thresholds for each technology.

3. Solar Potential

Since there is only one intermittent power source to supplement our system, the Sun, it is crucial to have a good estimate of the solar energy available for harvesting to appropriately size the power supply. This section discusses the method for obtaining the hourly solar irradiation on a surface using the PVGIS toolbox.

Before delving further, as presented in Figure 13, irradiance (W/m^2) or irradiation (Wh/m^2) can be broken down into three distinct components: direct, diffuse, and reflected. The direct component

refers to solar irradiation directly emitted from the Sun toward the solar harvesting surface. The diffuse component comprises solar irradiation, which scatters as it enters Earth's atmosphere before reaching the solar harvesting surface. Finally, there is the reflective component, which consists of solar irradiation that bounces off certain terrain elements. Typically, this last component can be ignored, except in scenarios that involve substantial snow or glassy surfaces. Note that the authors chose to take into account the influence of shadows created by the terrain and nearby obstacles. For complex shadows, please refer to our companion article "SolarImagingPy: An Affordable, Easy-to-Use Toolbox for Scientists to Predict Solar Potential in Partially Shaded Areas and Size Autonomous Power Supplies", where we provide a useful tool with a detailed guide to aid in the process of determining the solar irradiance available under environments with a lot of obstructions.

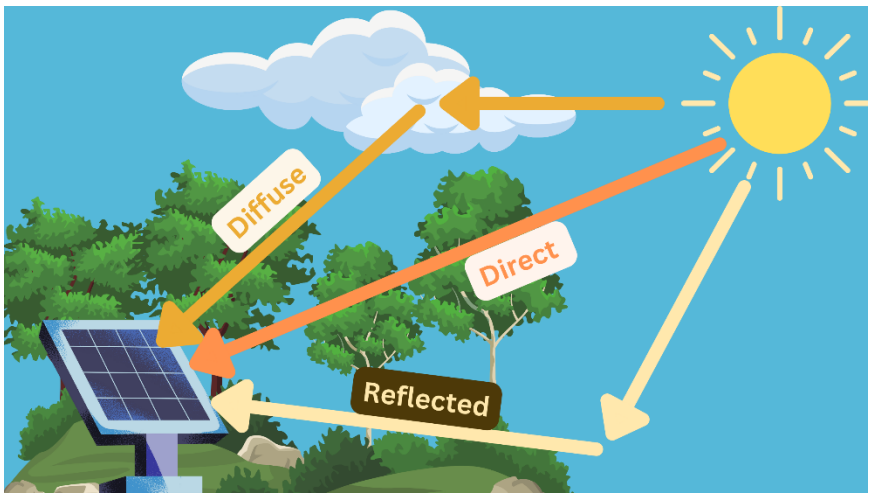

Figure 13. Illustration of three components that make up solar irradiation.

The amount of recovered solar energy depends on both the inclination and orientation of the solar panel.

The inclination denotes the tilt of the solar panel relative to the ground, while the orientation (or azimuth) signifies the cardinal direction the panel faces. The azimuth is measured clockwise from the south, with the south designated as 0°, the west as 90°, etc. In terms of inclination, the tilt is 0° when the panel is flat on the ground and 90° if the panel is perpendicular to the ground.

This section describes a step-by-step guide to retrieve a set of monthly PVGIS irradiation data.

1. Step 1 is to access the PVGIS interface (re.jrc.ec.europa.eu/pvg_tools) (accessed on 21 10 2024) and select the placement of the system on the map with the longitude and latitude of the site (Francon, a location near Toulouse, France for the chosen use case).
2. In Step 2, the user must select the section "Monthly data".
3. It is recommended that the user select the "Calculated horizon" on the right section selected, which is Step 3, as shown in Figure 14. This allows PVGIS to consider terrain elements (like mountains or hills) that could cause shadows and a loss of irradiation in the estimate. To consider shadows created by a house, a hedge (as for our system) or other simple shadow, a file describing these near shadows (by completing the site's skyline) can be added.
4. In Step 4, the first item of interest that the user should see is the "Solar radiation database", which the program decides by default. Next, the user must select the period of data to read from PVGIS (2010–2020, for example). Data are available for the period 2005 to 2020. Then, the user selects "Global irradiation at angle", then the azimuth is set to the south in 'monthly data' mode and the slope is set (0° in our case).
5. Step 5 involves ticking the "Visualize results" box so that PVGIS displays the monthly irradiation curve (Figure 15). This figure shows that the worst case corresponded to the month of December with 39 kWh/m². This value was divided by 31 to provide the daily irradiation Ir_{daily}^{dec} in winter (in Wh/m²), which is required for the initial sizing based on a daily balance.

In the second phase, the PVGIS software was used again (same place, fixed mounting option with azimuth and slope at 0°). To extract the hourly data, we changed "Monthly data" to "Hourly data", chose the duration (a 3-years period from 2010 to 2012, for example), and selected "Radiation components" before finally clicking on the csv button. A csv file was downloaded and was used for the hourly balancing budget presented in the section on hourly energy balance. This file contained the hourly three irradiation components that must be added before use.

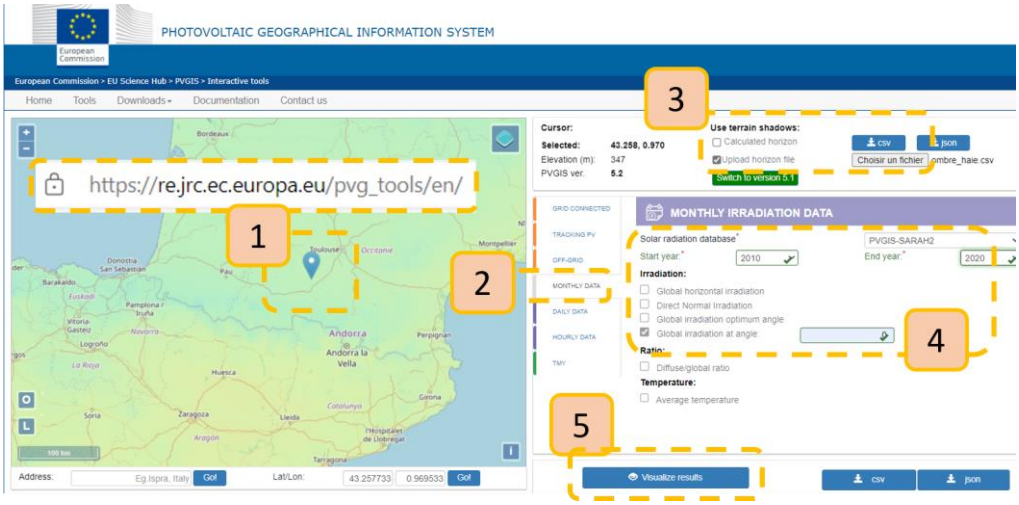

Figure 14. The PVGIS interface to retrieve the hourly irradiation data with the relevant items to consider for each step required to obtain an hourly solar irradiation estimate.

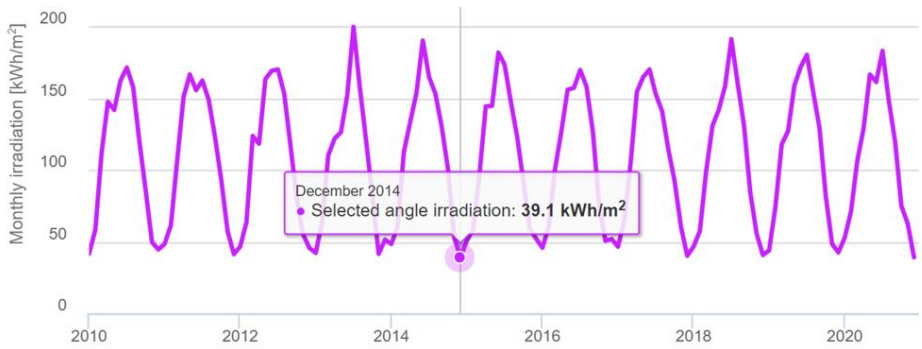

Figure 15. Monthly irradiation data over 10 years.

4. First Sizing

The objective was to find a PV surface S and the amount of energy embedded in the battery pack E_{bat}. This sizing uses **daily values** of **consumption** $E_{day}^{load} = 26$Wh and **irradiation** Ir_{daily}^{dec}. The solar power unit is described by the efficiency of the selected components, as presented in Figure 16.

η_{ch} is the ratio between the amount of electrochemical energy stored in the battery and the amount of electrical energy absorbed by the battery. Likewise, η_{dch} is the ratio of the amount of electrical energy delivered by the battery to the amount of electrochemical energy removed from the battery.

The battery charge efficiency η_{ch} was taken to be 0.7 for Pb and 0.8 for lithium-ion technologies. η_{dch} is generally close to 1. η_{MPPT} reflects the ability of the photovoltaic charger to make the panel work close to its maximum power point. Therefore, a value between 0.7 and 0.9 is appropriate. Let us denote the solar energy conversion efficiency as η_{pv}, the solar converter efficiency as η_1, and the load converter efficiency as η_2.

For both the PV regulator and the output regulator, an efficiency value of 0.8 is convenient without needing to delve into the specific specifications of the product used. For the sake of simplicity, we assumed that all of the energy leaving the solar charger was injected into the battery and that all of the energy consumed came from the battery (which strictly corresponds to an application with

storage during the day and consumption at night). Practically, this means that there was no power running along the orange dotted path in Figure 16. This last situation will be considered in the next paragraph with the hourly simulation.

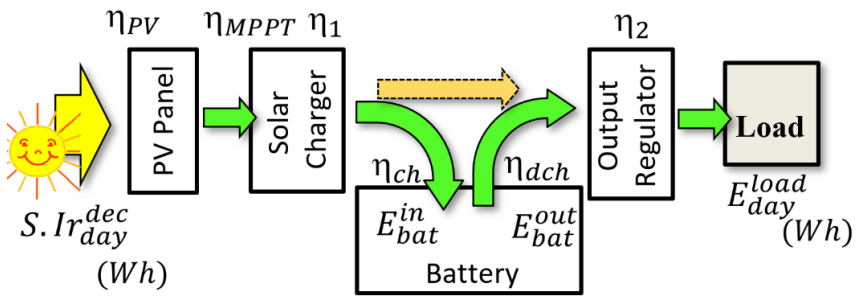

Figure 16. Efficiency of the energy chain.

The maximum amount of energy stored in the battery per day E_{bat}^{in} then corresponds to the energy supplied by the Sun, affected by the efficiency of part of the conversion chain, in other words:

$$\left(S.Ir_{day}^{dec}\right).\eta_{PV}.\eta_{MPPT}.\eta_1.\eta_{ch} = E_{bat}^{in} \quad (8)$$

On the consumption side, per day, the battery delivers E_{bat}^{out} to supply the load.

$$E_{bat}^{out}.\eta_{dch}.\eta_2 = E_{day}^{load} \quad (9)$$

If the surface area S is chosen to compensate for consumption, then we have:

$$E_{bat}^{in} = E_{bat}^{out} \quad (10)$$

Using Equation (8) to Equation (10):

$$S = \frac{E_{day}^{load}}{Ir_{day}^{dec}.(\eta_{PV}.\eta_{MPPT}.\eta_1.\eta_{ch}.\eta_{dch}.\eta_2)} \quad (11)$$

This gives a panel surface that is suitable even during periods of bad weather.

$S = 0.3\ m^2$ is convenient for the chosen application and was exactly the size of the chosen PV panel.

To size the battery, a DoD_{Max} value of 60% was chosen to ensure the battery's longevity (SOC_{Min} = 40%).

To obtain sunshine information, the hourly mean irradiation data were aggregated to provide the daily irradiation data. Figure 17a shows the daily irradiation over 3 years. The least favorable period was December–January, with an average of 1.26 kWh/day/m². If we assume that there is no recharging on days when the irradiation is below this value, zooming in on Figure 17a, we find N = 2 consecutive days of complete autonomy without any solar recharging, which is a reasonable value to complete the sizing.

The battery should then provide E'_{out}, according to Equation (10):

$$E'_{out} = \frac{N.E_{day}^{load}}{\eta_{dch}.\eta_2} \quad (12)$$

By definition,

$$DoD_{Max} = \frac{E'_{out}}{E_{bat}} \quad (13)$$

Thus,

$$E_{bat} = \frac{N.E_{day}^{load}}{DoD_{Max}.\eta_{dch}.\eta_2} \quad (14)$$

This leads to a value of $E_{bat} =$ 125 Wh, in accordance with the chosen value (112 Wh).

It should be noted that for users in a hurry, PVGIS offers an Off-Grid tab that allows for an initial dimensioning of the PV system to be quickly obtained with the minimum information.

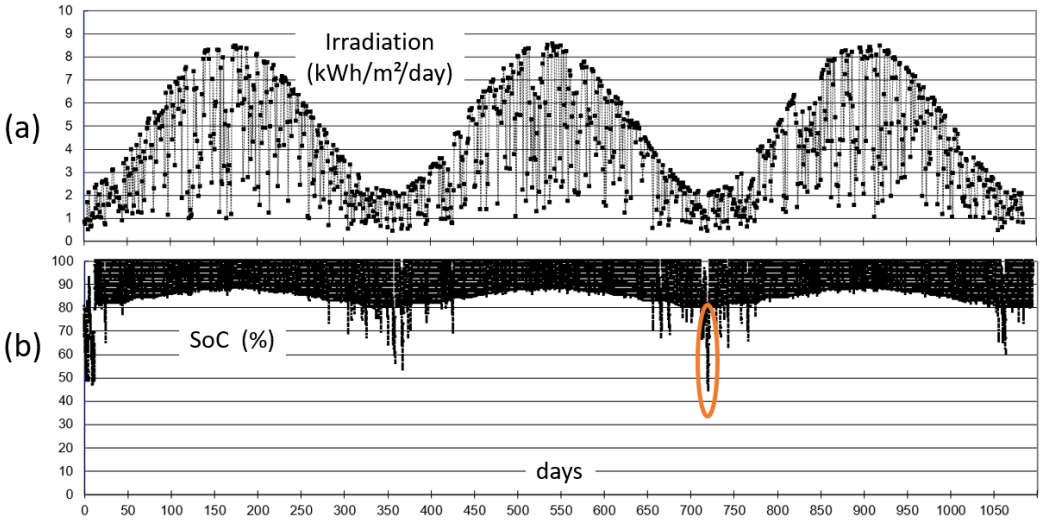

Figure 17. (**a**) Daily irradiation between 01/01/2010 and 31/12/2012. (**b**) Hourly battery state of charge (SoC) obtained with S = 0.24 m² and $Ebat$ = 112 Wh.

5. Hourly Energy Balance

Hourly simulations of the state of charge of the battery indicate the amount of energy available in the system. It is of great interest for determining whether the system is properly sized or not. Before going into the simulation, it is important to remind the reader that at this point, we had already determined the hourly solar irradiation, the hourly energy consumption, and for the solar power unit, a set of selected components, previously described by their efficiency.

Let us consider the following variables: solar energy irradiation I_{solar}^{h} available at hour h, the energy consumed E_{load}^{h} by the load at hour h, and the energy flow into or out of the battery ΔE_{bat}^{h} by the load at hour h. Each hour, the amount of energy leaving the PV regulator is:

$$E_A = S.I_{solar}^{h}.\eta_{MPPT}.\eta_{pv}.\eta_1 \tag{15}$$

and the energy fed into the output regulator is

$$E_B = E_{load}^{h}/\eta_2 \tag{16}$$

A positive difference means that the battery is charging; otherwise, it is discharging. If we note ΔE_{bat}^{h} the variation in energy each hour, the hourly balance is:

$$\Delta E_{bat}^{h} = \begin{cases} \eta_{ch}.(E_A - E_B) & if \;\; E_A - E_B \geq 0 \\ \dfrac{(E_A - E_B)}{\eta_{dch}} & if \;\; E_A - E_B < 0 \end{cases} \tag{17}$$

The spreadsheet can then be used to determine the energy level at the end of the hour (Equation (18)) and the state of charge (Equation (19)).

$$E_{bat}^{h+1} = \begin{cases} E_{bat}^{h} + \Delta E_{bat}^{h} & if \;\; 0 < E_{bat}^{h} + \Delta E_{bat}^{h} < C.V_{bat} \\ C.V_{bat} & if \;\; E_{bat}^{h} + \Delta E_{bat}^{h} \geq C.V_{bat} \\ 0 & if \;\; E_{bat}^{h} + \Delta E_{bat}^{h} \leq 0 \end{cases} \tag{18}$$

$$SoC^{h+1} = \frac{E_{bat}^{h+1}}{C.V_{bat}} \tag{19}$$

The result is the hourly state of charge for the period in question, as illustrated in Figures 17b and 18 with the optimal sizing, which must remain above the minimum authorized value. If this is not the case, the user can restart the simulation with a greater PV panel area or more energy stored in the battery until a suitable set of parameters is obtained. A safety margin of 20% on the PV surface is traditionally used to account for exceptional weather conditions. The part circled in orange in Figure 17b is enlarged in Figure 18 and shows what happens when one of the parameters is modified, for example, reducing the solar panel by 20% to 0.24 m^2 instead of the initial value of 0.3 m^2 brought the SOC just close to the acceptable limit in winter (40%). The red curve in Figure 18 shows the direct correlation between the lack of irradiance and the reduction in the battery's state of charge.

Finally, the first design was validated by both the hourly simulation and in practice after a year's operation with no supply problems.

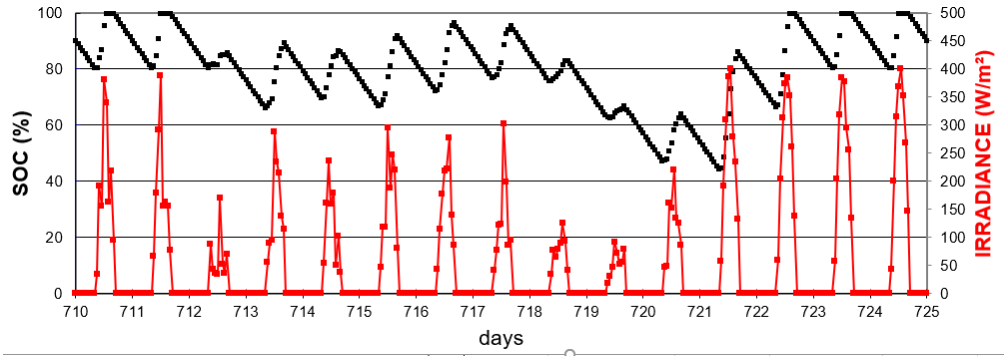

Figure 18. Black curve: battery SoC (%) between 11/12/2011 (day 710) and 25/12/2011, results obtained with S = 0.24 m^2, *Ebat* = 112 Wh. Red curve: average hourly irradiance (W/m^2).

6. Component Selection

Once the power of the PV panel has been fixed, the choice of the open-circuit voltage is important. An analysis of the small- and medium-size photovoltaic generator on the market shows:

1. A first series of products with power ratings between 0.5 and 14 W, with open circuit voltages between 5 and 8 V and short circuit currents between 0.1 and 2 A.
2. A second series of more powerful products, between 10 and 50 W, with an open circuit voltage between 18 and 22 V for short circuit currents between 0.6 and 3 A.
3. Some products based on large whole solar cells (SunPower Maxeon cells) or half-cells with low voltages but high current (3 to 6 A)

The first series is well-suited to a 1S (3.6 V) battery structure with an interposed buck solar inverter, or to a 2S (7.2 V) battery structure with buck or buck-boost solar inverters. A buck, boost, or buck-boost converter is then placed downstream of the battery to produce 5 V or 3.3 V, depending on the output voltage required by the load.

For the second series, a solar buck converter is convenient with a 3S or 4S lithium battery (10.8 V or 14.4 V, respectively) or a 12 V lead battery. A PWM regulator is also suitable in this case. The converter downstream of the battery will then generally be a buck for a 12 or 5 V load. Lower voltages should be avoided as this will reduce the global efficiency.

For the third series, a boost converter with MPPT function is often chosen.

Finally, the required capacity of the battery can be deduced using Equation (6) from the battery energy previously validated by the simulation and from the chosen battery voltage.

In all cases, it is crucial to check that the input and output currents do not surpass the specifications of the product.

7. Conclusions

In this article, we have summarized a simple and comprehensive procedure for sizing an autonomous solar power supply that is appropriate for a given location and use. The method works for sites in full sun with no shading, but it also takes into account distant shading (hills) or shading easily described by a continuous horizon line (clearing, forest edge, building). We have also presented

various examples of commercial products for consideration. The proposed design was successfully validated experimentally on one site over a full year. By presuming a fundamental understanding of electrical concepts, we have ensured that the procedure is accessible to a broad audience. Nonetheless, this work assumes the absence of complex obstructions in close proximity to the deployed solar panels, and this assumption may not be applicable to many field applications. Consequently, we have developed a companion work, "SolarImagingPy: An Affordable, Easy-to-Use Toolbox for Scientists to Predict Solar Potential in Partially Shaded Areas and Size Autonomous Power Supplies." This free and open-source toolbox was created to assist researchers in more accurately estimating the solar irradiance under complex shading conditions.

Author Contributions: Conceptualization, V.B., K.B.K.C., and B.E.; Methodology, V.B., K.B.K.C., B.E., and A.E.; Software, V.B. and K.B.K.C.; Validation, All authors; Investigation, V.B., K.B.K.C., A.E., and J.-L.D.; Writing—original draft preparation, V.B., K.B.K.C., and B.E.; Writing—review and editing, V.B., K.B.K.C. and A.E.; Visualization, All authors; Supervision, V.B. All authors have read and agreed to the published version of the manuscript.

Funding: This work was funded by the European Regional Development Fund (project ECONECT), by the Region Occitanie / Pyrénées-Méditerranée (project DIAGNOSE) and by the French National Program (ANR) "Investment for Future-Excellency Equipment" (project TERRA FORMA, with the reference ANR-21-ESRE-0014). M.C is funded by the Junior Professor Chair NeoSensation (ANR-23-CPJ1-0174-01)

References

4. Besson, M.; Alison, J.; Bjerge, K.; Gorochowski, T.E.; Høye, T.T.; Jucker, T.; Mann, H.M.R.; Clements, C.F. Towards the fully automated monitoring of ecological communities. *Ecol. Lett.* **2022**, *25*, 2753–2775. https://doi.org/10.1111/ele.14123.
5. Mabon, M.; Gautier, M.; Vrigneau, B.; Le Gentil, M.; Berder, O. The Smaller the Better: Designing Solar Energy Harvesting Sensor Nodes for Long-Range Monitoring. *Wirel. Commun. Mob. Comput.* **2019**, *2019*, 2878545. https://doi.org/10.1155/2019/2878545.
6. Tsiropoulos, Z.; Gravalos, I.; Skoubris, E.; Poulek, V.; Petrík, T.; Libra, M. A Comparative Analysis between Battery- and Solar-Powered Wireless Sensors for Soil Water Monitoring. *Appl. Sci.* **2022**, *12*, 1130. https://doi.org/10.3390/app12031130.
7. Varadharajan, C.; Faybishenko, B.; Henderson, A.; Henderson, M.; Hendrix, V.C.; Hubbard, S.S.; Kakalia, Z.; Newman, A.; Potter, B.; Steltzer, H.; et al. Challenges in Building an End-to-End System for Acquisition, Management, and Integration of Diverse Data From Sensor Networks in Watersheds: Lessons From a Mountainous Community Observatory in East River, Colorado. *IEEE Access* **2019**, *7*, 182796–182813. https://doi.org/10.1109/ACCESS.2019.2957793.
8. Zhang, Z.; Glaser, S.; Watteyne, T.; Malek, S. Long-Term Monitoring of the Sierra Nevada Snowpack Using Wireless Sensor Networks. *IEEE Internet Things J.* **2022**, *9*, 17185–17193. https://doi.org/10.1109/JIOT.2020.2970596.
9. Filhol, S.; Lefeuvre, P.-M.; Ibañez, J.D.; Hulth, J.; Hudson, S.R.; Gallet, J.-C.; Schuler, T.V.; Burkhart, J.F. A new approach to meteorological observations on remote polar glaciers using open-source internet of things technologies. *Front. Environ. Sci.* **2023**, *11*. Available online: https://www.frontiersin.org/articles/10.3389/fenvs.2023.1085708 (accessed on 2 February 2024).
10. Kasama, T.; Koide, T.; Bula, W.P.; Yaji, Y.; Endo, Y.; Miyake, R. Low Cost and Robust Field-Deployable Environmental Sensor for Smart Agriculture. In Proceedings of the 2019 2nd International Symposium on Devices, Circuits and Systems (ISDCS), Higashi-Hiroshima, Japan, 6–8 March 2019; pp. 1–4. https://doi.org/10.1109/ISDCS.2019.8719262.
11. Jolles, J.W. Broad-scale applications of the Raspberry Pi: A review and guide for biologists. *Methods Ecol. Evol.* **2021**, *12*, 1562–1579. https://doi.org/10.1111/2041-210X.13652.
12. Petrariu, A.I.; Lavric, A.; Coca, E.; Popa, V. Hybrid Power Management System for LoRa Communication Using Renewable Energy. *IEEE Internet Things J.* **2021**, *8*, 8423–8436. https://doi.org/10.1109/JIOT.2020.3046324.
13. Fendzi, W.M.; Dzonde, S.R.N.; Molu, R.J.J.; Tsobze, S.K. Contribution into Robust Optimization of Renewable Energy Sources: Case Study of a Standalone Hybrid Renewable System in Cameroon. *Int. J. Renew. Energy Res. IJRER* **2023**, *13*, 1093–1120.
14. Proppe, D.S.; Pandit, M.M.; Bridge, E.S.; Jasperse, P.; Holwerda, C. Semi-portable solar power to facilitate continuous operation of technology in the field. *Methods Ecol. Evol.* **2020**, *11*, 1388–1394. https://doi.org/10.1111/2041-210X.13456.
15. Photovoltaics, D.G.; Storage, E. *IEEE Recommended Practice for Sizing Stand-Alone Photovoltaic (PV) Systems*; IEEE: 2021. https://doi.org/10.1109/IEEESTD.2021.9528316.

16. Ali, M.F.M.; Ibrahim, A.A.; Zaman, M.H.M. Optimal Sizing of Solar Panel and Battery Storage for A Smart Aquaponic System. In Proceedings of the 2021 IEEE 19th Student Conference on Research and Development (SCOReD), Kota Kinabalu, Malaysia, 23–25 November 2021; pp. 186–191. https://doi.org/10.1109/SCOReD53546.2021.9652782.
17. Zhang, Y.; Wetherill, B.R.; Chen, R.F.; Peri, F.; Rosen, P.; Little, T.D.C. Design and implementation of a wireless video camera network for coastal erosion monitoring. *Ecol. Inform.* **2014**, *23*, 98–106. https://doi.org/10.1016/j.ecoinf.2013.07.003.
18. Manchev, N.P.; Angelov, K.K.; Karapenev, B.D. Energy Performance Analysis of LoRaWAN End Device with Autonomous Power Supply. In Proceedings of the 2022 XXXI International Scientific Conference Electronics (ET), Sozopol, Bulgaria, 13–15 September 2022; pp. 1–6. https://doi.org/10.1109/ET55967.2022.9920213.
19. Craciunescu, D.; Fara, L. Investigation of the Partial Shading Effect of Photovoltaic Panels and Optimization of Their Performance Based on High-Efficiency FLC Algorithm. *Energies* **2023**, *16*, 1169. https://doi.org/10.3390/en16031169.
20. Zhang, Y.; Feng, X.; Chang, X.; Tie, L. Impacts of canopy structure on the sub-canopy solar radiation under a deciduous forest based on fisheye photographs. *Res. Cold Arid Reg.* **2023**, *15*, 150–160. https://doi.org/10.1016/j.rcar.2023.06.005.
21. Cao, K.B.K. Photovoltaic Applications in Demanding Situations: Estimation and Optimisation of Solar Ressources for Autonomous Power Supplies. Ph.D. Thesis, Toulouse, France INSA, 2023. Available online: https://theses.fr/2023ISAT0027 (accessed on 21 10 2024).
22. Marion, W.; Wilcox, S. Solar Radiation Data Manual for Flat-Plate and Concentrating Collectors; NREL/TP-463-5607, 10169141, ON: DE93018229; National Renewable Energy Laboratory (NREL): Golden, CO, USA, 1994. https://doi.org/10.2172/10169141.
23. Park, S.-J.; Song, Y.-W.; Kang, B.-S.; Kim, W.-J.; Choi, Y.-J.; Kim, C.; Hong, Y.-S. Depth of discharge characteristics and control strategy to optimize electric vehicle battery life. *J. Energy Storage* **2023**, *59*, 106477. https://doi.org/10.1016/j.est.2022.106477.